TUTORIAL

Cold bosons in optical lattices: a tutorial for exact diagonalization

To cite this article: David Raventós *et al* 2017 *J. Phys. B: At. Mol. Opt. Phys.* **50** 113001

View the article online for updates and enhancements.

Related content

- Generation of atypical hopping and interactions by kinetic driving
  G Pieplow, F Sols and C E Creffield

- Non-standard Hubbard models in optical lattices: a review
  Omjyoti Dutta, Mariusz Gajda, Philipp Hauke et al.

- Fragmented condensation in Bose–Hubbard trimers with tunable tunnelling
  A Gallemí, M Guilleumas, J Martorell et al.

Recent citations

- On continuum model analog to zig-zag optical lattice in quantum optics
  M. Tantawy and H. I. Abdel-Gawad

- Static properties of two linearly coupled discrete circuits
  Albert Escrivà *et al*

- Topological end states in a one-dimensional spatially modulated interaction spinless fermion model
  Zheng-Wei Zuo *et al*

Tutorial

Cold bosons in optical lattices: a tutorial for exact diagonalization

David Raventós[1,6]**, Tobias Graß**[1,2]**, Maciej Lewenstein**[1,3] **and Bruno Juliá-Díaz**[1,4,5]

[1] ICFO-Institut de Ciencies Fotoniques, The Barcelona Institute of Science and Technology, 08860, Castelldefels (Barcelona), Spain
[2] Joint Quantum Institute, University of Maryland, College Park, MD 20742, United States of America
[3] ICREA, Passeig de Lluís Companys, 23, 08010 Barcelona, Spain
[4] Departament de Física Quàntica i Astrofísica, Facultat de Física, Universitat de Barcelona, Barcelona E-08028, Spain
[5] Institut de Ciències del Cosmos, Universitat de Barcelona, ICCUB, Martí i Franquès 1, Barcelona E-08028, Spain

E-mail: david.raventos@icfo.eu

Abstract

Exact diagonalization (ED) techniques are a powerful method for studying many-body problems. Here, we apply this method to systems of few bosons in an optical lattice, and use it to demonstrate the emergence of interesting quantum phenomena such as fragmentation and coherence. Starting with a standard Bose–Hubbard Hamiltonian, we first revise the characterisation of the superfluid to Mott insulator (MI) transitions. We then consider an inhomogeneous lattice, where one potential minimum is made much deeper than the others. The MI phase due to repulsive on-site interactions then competes with the trapping of all atoms in the deep potential. Finally, we turn our attention to attractively interacting systems, and discuss the appearance of strongly correlated phases and the onset of localisation for a slightly biased lattice. The article is intended to serve as a tutorial for ED of Bose–Hubbard models.

Keywords: many-body problems, cold bosons, optical lattices

(Some figures may appear in colour only in the online journal)

1. Introduction

The Bose–Hubbard model (BHM), originally introduced in order to describe different phenomena in condensed matter physics [1], has gained new impact in the field of quantum gases [2], following the experimental realisation of the model in a setup with cold atoms in optical lattices [3]. In particular, the prediction of a phase transition from a superfluid (SF) to a Mott insulator (MI) has been confirmed. The origin of this transition is genuinely quantum, that is, it is driven by quantum fluctuations, which are controlled by the Hamiltonian parameters, interaction and hopping strength, and which are present also at zero temperature.

The advantages offered by cold atoms for studying quantum phase transitions are clear. First, in these systems, high isolation from the surrounding environment is achievable. There have been recent advances in producing different sort of lattice configurations, determining the Hamiltonian parameters. Second, atom–atom interactions are tunable via Feshbach resonances. These properties allow one to use ultracold atomic systems as quantum simulators of theoretical models that are not tractable with classical computers. Although different techniques are able to capture ground state properties of the Bose–Hubbard Hamiltonian, the solution of

---

[6] Author to whom any correspondence should be addressed.

J. Phys. B: At. Mol. Opt. Phys. **50** (2017) 113001

Tutorial

the full model, that is complete spectrum and eigenstates, appears to be intractable with classical techniques. Exact diagonalization (ED) techniques, which in principle allow one to solve the full problem with high accuracy, suffer from the clear shortcoming of being restricted to fairly small many-body quantum systems [4].

Several approaches have been used to study the BHM: Bogoliubov techniques at small interactions [5], perturbative ones at large interactions [6, 7], Gutzwiller mean-field approaches [8, 9], field-theoretic studies [10–12], etc. Ground state properties can be studied by means of DMRG methods [13, 14] and quantum Monte-Carlo techniques [15].

While the phase boundary between the Mott insulating phase and the SF phase is well-defined in the thermodynamic limit, where symmetry-breaking gives rise to a non-zero order parameter, the situation is less unique for finite systems. In particular, as reviewed in [16] and also pointed out in [14], there is still uncertainty on the precise value of the transition from Mott to SF in 1D systems. In particular quantum Monte-Carlo studies have produced slightly disagreeing results on the critical value of the parameters [17–19]. In view of this, further study of the Mott transition is needed, using different techniques and applying different definitions. Here, exact methods allow to extract quantities not reachable by means of other methods, such as eigenstates, eigenenergies and the Entanglement spectrum.

In this work we consider small lattices which we study using ED. We apply and compare different signatures of the MI-SF transition: given the full ground state of the system, a simple figure of merit is the overlap between the numerical solution and analytical trial states for the Mott and the SF phase. To capture the phase boundary more accurately, we extract the single-particle insulating gap from the energy spectra at different numbers of atoms. Performing a finite size scaling, we determine the parameters for which the gap would close in the thermodynamic limit, indicating the transition to the SF phase.

Interesting new phenomena are brought into the problem by a simple modification of the model, assuming a lattice with one highly biased site attracting the atoms. This gives rise to a series of quantum phase transitions upon changing the lattice depth: For certain values, number fluctuations in the system become strong while the average number of particles on the biased site is decreased by one.

Finally, we consider the case of attractive interactions. Similarly to the two-site case discussed in [20, 21], strong fragmentation is found in the ground state of the system for a small attractive interaction. Direct diagonalization allows us to quantitatively discuss the appearance of many-body correlations in the ground state. Considering a slightly biased lattice, we study the onset of localisation in the system as the attraction is increased.

The present manuscript is also intended to provide a detailed, tutorial like, description of the methods employed to perform the ED of the model. Our work complements other tutorial like ones, like [22], as we also incorporate a state-of-the-art discussion of the definition of the transition between the MI and SF phases.

This work is organised as follows: the BHM is introduced in section 2. In section 2.1, we introduce different quantities used to characterise the system behaviour, such as eigenvalues of the one body density matrix, and the populations of the Fock states. They allow us to discern if the system is condensed and to measure its spatial correlations. We also define different entropies in order to capture important properties about the system with a single scalar value. In section 2.2, we present the phases exhibited by the BHM. In section 3 we explain the ED techniques used together with a detailed description of how to perform them. In section 4 we present the U/t value at which the MI-SF phase transition takes place for the BHM at filling 1, applying several finite size studies to our ED results. In section 5, we go beyond the standard BHM: In section 5.1, we study an inhomogeneous lattice, and observe several transitions as the hopping and/or interaction strengths are varied, and in section 5.2, we turn to attractive interactions, focusing on the appearance of correlated states. In section 5.3, the reader is briefly introduced to the treatment of quantum Hall effects with ED. Conclusions are given in section 6.

2. The BHM and its characterisation

We start considering the standard BHM which contains two terms: the hopping term, which allows the exchange of particles between the sites, related to the kinetic energy, and the on-site interaction term, which can be repulsive or attractive. The Hamiltonian of the model reads,

$$\hat{\mathcal{H}} = -\sum_{j \neq k}^{M} t_{k,j} \hat{a}_j^\dagger \hat{a}_k + \frac{U}{2} \sum_{i=1}^{M} \hat{n}_i (\hat{n}_i - 1)$$
$$\equiv \sum_{j \neq k}^{M} \hat{\mathcal{T}}_{k,j} + \sum_{i=1}^{M} \hat{\mathcal{U}}_i, \tag{1}$$

where $\hat{a}_j^\dagger$ ($\hat{a}_j$) creates (annihilates) one particle in the jth site and $\hat{n}_i = \hat{a}_i^\dagger \hat{a}_i$ is the number of particles operator in the ith site, being M the number of sites. A convenient finite basis, with a fixed number of particles N, is given by the states of the Fock space restricted to N particles,

$$|\beta\rangle \equiv |n_1^\beta, n_2^\beta, \cdots, n_M^\beta\rangle \equiv \frac{1}{\sqrt{n_1! n_2! \ldots n_M!}}$$
$$\times (\hat{a}_1^\dagger)^{n_1} (\hat{a}_2^\dagger)^{n_2} \ldots (\hat{a}_M^\dagger)^{n_M} |\text{vac}\rangle, \tag{2}$$

where n_i^β is the number of bosons at the ith site in the state $|\beta\rangle$, and β is the labelling of the Fock states. Since the number of bosons N in the system is fixed, n_i^β satisfies $\sum_i^M n_i^\beta = N$ for any state $|\beta\rangle$. Arbitrary states can be written in this orthogonal basis,

$$|\Phi\rangle = \sum_\beta^{\mathcal{N}_N^M} c_\beta |\beta\rangle, \tag{3}$$

with $c_\beta \in \mathbb{C}$. For total number of bosons N and sites M there are $\mathcal{N}_N^M$ Fock states in the basis. This number is the number of

Table 1. Size of the Hilbert space for N bosons in M sites, $\mathcal{N}_N^M$ for $N, M = 1, \ldots, 13$.

							M						
N	1	2	3	4	5	6	7	8	9	10	11	12	13
1	1	2	3	4	5	6	7	8	9	10	11	12	13
2	1	3	6	10	15	21	28	36	45	55	66	78	91
3	1	4	10	20	35	56	84	120	165	220	286	364	455
4	1	5	15	35	70	126	210	330	495	715	1001	1365	1820
5	1	6	21	56	126	252	462	792	1287	2002	3003	4368	6188
6	1	7	28	84	210	462	924	1716	3003	5005	8008	12376	18564
7	1	8	36	120	330	792	1716	3432	6435	11440	19448	31824	50388
8	1	9	45	165	495	1287	3003	6435	12870	24310	43758	75582	125970
9	1	10	55	220	715	2002	5005	11440	24310	48620	92378	167960	293930
10	1	11	66	286	1001	3003	8008	19448	43758	92378	184756	352716	646646
11	1	12	78	364	1365	4368	12376	31824	75582	167960	352716	705432	1352078
12	1	13	91	455	1820	6188	18564	50388	125970	293930	646646	1352078	2704156
13	1	14	105	560	2380	8568	27132	77520	203490	497420	1144066	2496144	5200300

ways of placing N particles in M sites, see table 1,

$$\mathcal{N}_N^M = \binom{N+M-1}{N} = \frac{(N+M-1)!}{N!(M-1)!}. \qquad (4)$$

If the particles were fermions instead of bosons, the number of basis states is,

$$\mathcal{N}_N^{M,\text{fermions}} = \binom{M}{N}. \qquad (5)$$

2.1. Useful quantities

Let us introduce some quantities that we will use in this work to discuss the characterisation of the BHM.

2.1.1. Fragmentation in the ultracold gas. The generalisation of the concept of Bose–Einstein condensation to interacting systems was introduced by Penrose and Onsager [23, 24]. They established a condensation criterion in terms of the one-body density matrix (OBDM),

$$\rho^{(1)}(\mathbf{r}, \mathbf{r}') = \langle \psi^\dagger(\mathbf{r}')\psi(\mathbf{r}) \rangle, \qquad (6)$$

where the field operator $\psi^\dagger$ creates a boson at position $\mathbf{r}$ and $\langle \cdots \rangle$ is the thermal average at temperature T. Since $\rho^{(1)}$ is a Hermitian matrix, it can be diagonalized. The eigenvectors are termed natural orbitals, and the eigenvalues are their corresponding populations.

The way to find out if a given state is condensed involves the computation of the OBDM and its diagonalization in order to study the size of the populations of its eigenstates. In second quantisation, the definition of the OBDM $\rho_{k,l}$ of a state $|\Phi\rangle$ is,

$$\rho_{k,l} = \langle \Phi | \hat{a}_l^\dagger \hat{a}_k | \Phi \rangle. \qquad (7)$$

But writing the state $|\Phi\rangle$ as in equation (3), we explicitly get,

$$\rho_{k,l} = \sum_{\alpha,\beta}^{\mathcal{N}_N^M} c_\alpha^* c_\beta \langle \alpha | \hat{a}_l^\dagger \hat{a}_k | \beta \rangle. \qquad (8)$$

From the diagonalization of the OBDM in an arbitrary basis, one obtains,

$$\rho_{i,j} = n_i^{\text{OBDM}} \delta_{i,j}, \qquad (9)$$

where n_i^{OBDM} is the ith largest eigenvalue of the OBDM.

In order to simplify the information given by the eigenvalues of the OBDM of a given state, we introduce an entropy based on the von Neumann one, S_1, which will be used in the following. It is defined as,

$$S_1 = -\sum_i^M p_i \ln p_i, \qquad (10)$$

with $p_i = n_i^{\text{OBDM}}/N$ the normalised eigenvalues of the OBDM. So, $\sum_i p_i = 1$. The minimum of S_1 is 0 and corresponds to $p_i = \delta_{i,1}$. The entropy S_1 has a maximum which equals $\ln M$ when $p_i = 1/M$, $\forall i$. So, its maximum value corresponds to a uniform probability distribution (fragmented condensate [25]), whereas the minimum corresponds to a Kronecker-δ distribution, full condensation. In all computations, the entropy has been divided by its maximum value, $\ln M$, in order get a non-extensive quantity, bounded by 0 and 1.

The entropy S_1 measures condensation, as defined by the Penrose-Onsager criterion. When the value is 0, the system is condensed. When it is $\ln M$, it is completely fragmented. When the value is the logarithm of a certain integer r, the state is fragmented in r states.

2.1.2. Spatial correlations from Fock-space coefficients. In order to quantify the correlations between the particles on different sites, we take advantage from the fact that our Fock basis builds on spatially localised single particle states. We define a second entropy S_D, which measures the clustering of particles in the Fock space,

$$S_D = -\sum_\beta^{\mathcal{N}_N^M} |c_\beta|^2 \ln |c_\beta|^2, \qquad (11)$$

J. Phys. B: At. Mol. Opt. Phys. **50** (2017) 113001

Tutorial

where c_β are the coefficients of the decomposition of a given state into the Fock basis $|\beta\rangle$, equation (3). In the same way as the entropy S_1 allowed us to distinguish between condensed and fragmented states, the entropy S_D distinguishes between many-body states which are represented by a single Fock state ($S_D = 0$), and superpositions of many Fock states ($S_D > 0$). Apparently, if only few Fock states contribute to a many-body state, there is a high amount of spatial correlations in the system, which thus can be captured by the value of S_D. The entropy S_D is the von Neumann entropy of the diagonal ensemble after tracing off one site. This means that it provides the von Neumann entropy after a long-term time evolution in a local Hamiltonian $\hat{\mathcal{H}} = \sum_i \epsilon_i \hat{n}_i$, with ϵ_i local energies. Note that in the case of solely two-sites, the entropy S_D coincides with the left–right bipartite entropy [21].

2.2. Phases of the BH model

The homogeneous case of the Hamiltonian (1), with $t_{k,j} = t$, becomes exactly solvable in two limiting cases: $t/U = 0$ and $t/U \to \infty$. We take ground states in these two cases as analytical trial states for the two quantum phases exhibited by the model: the non-interacting limit provides a trial state for the SF phase, while the system without hopping yields a trial state for the MI phase.

2.2.1. MI regime.
When $t/U \to 0$ with $U > 0$, the system is dominated by the repulsive interactions, and it minimises energy by reducing the number of pairs in each site. So, the GS of the system is a state with $q \equiv N/M$ particles on each site, where q is a positive integer, i.e., a MI state. This corresponds to one many-body state of the Fock basis and it reads,

$$|\Phi_{\text{MI}}(q)\rangle = \prod_{i=1}^{M} \frac{(\hat{a}_i^\dagger)^q}{\sqrt{q!}}|0\rangle = |q \cdots q\rangle. \quad (12)$$

The first excited state looks like a MI state where a particle has been annihilated in one site and created in a different site, i.e., it is a quasiparticle–quasihole excitation of the MI state. When the particle is created in the ith site and the hole is localised in the jth one, the first excited state reads,

$$|\Phi_{\text{MI}}(q)\rangle^{(1)} = \frac{1}{q}\hat{a}_i^\dagger \hat{a}_j |\Phi_{\text{MI}}(q)\rangle. \quad (13)$$

The MI is an insulator in the sense that the 'transport' of one particle from one site to another costs a finite amount of energy (the energy gap ΔE). In the MI state, when q particles are in one site, the value of the interaction term in that site is $(U/2)q(q-1)$. When in the MI state, a particle hops from one site to another, the value on the interaction term is $(U/2)(q-1)(q-2)$ in the site where the particle comes from and $(U/2)(q+1)q$ in the site where the particle goes. This situation coincides with the first excitation of the MI state. So, the energy difference of the MI state and its

excitation is,

$$\Delta E = \frac{U}{2}[(q-1)(q-2) + (q+1)q - 2q(q-1)] = U. \quad (14)$$

Thus, the MI phase has a characteristic energy gap $\Delta E = U$ in the energy spectrum which separates the ground state from the excitations.

We consider systems at filling one, that is, $q = N/M = 1$. In the MI phase, there is one particle in each site and $S_1 = \log M$. Due to the fact that in this phase the GS coincides with a single Fock state, S_D is zero. Since the number of particles q in each site is a well-defined integer, there are no fluctuations on the on-site number of particles in the Mott phase. The MI phase also has a finite correlation length ξ, defined in $\langle a_i a_j \rangle - \langle a_i \rangle \langle a_j \rangle \propto e^{-|\mathbf{r}_i - \mathbf{r}_j|/\xi}$ as a measure of the spatial range of pair correlations.

2.2.2. SF regime.
When $U/t \to 0$, the hopping rules the system and each particle becomes completely delocalised over all sites of the lattice. So, we can write the single particle state as,

$$|\phi_{\text{sp}}\rangle = \frac{1}{\sqrt{M}}\sum_{i=1}^{M}\hat{a}_i^\dagger|0\rangle. \quad (15)$$

Since there are no interactions, the state of the whole system is a properly symmetrized product of the single particle state up to the number of particles. So,

$$|\Phi_{\text{SF}}\rangle = \frac{1}{\sqrt{N!}}\left[\frac{1}{\sqrt{M}}\sum_{i=1}^{M}\hat{a}_i^\dagger\right]^N|0\rangle. \quad (16)$$

Then, the squared coefficients of the decomposition of the SF state into the Fock basis follow a poissonian distribution in the sense that its variance $\text{Var}(|c_\beta|^2)$ coincides with its mean $\langle|c_\beta|^2\rangle$ [3].

The SF state is characterised by a vanishing gap (since there is no interaction, the only contribution to the gap comes from the hopping term), large fluctuations in the on-site number of particles and a divergent correlation function. In the SF phase, all particles are delocalised, that is, each one of them has the same probability of presence in all sites of the lattice, without interacting with each other. Since all the particles in the system have the same single particle wavefunction, the system is condensed and so, $S_1 = 0$. The SF state involves many Fock states with a non-uniform distribution. The entropy S_D, defined in equation (11), is larger than in the Mott phase, but it will never equal 1 because the distribution is not uniform. Increasing the number of particles in the system, the value of the entropy S_D in the SF phase decreases. In contrast to S_1, the entropy S_D does not exhibit an extremal value. In section 5, we will encounter cases where the distribution of coefficients is closer to a uniform distribution, giving rise to even larger values of S_D.

3. Exact diagonalization

Let us depiece how we have performed the ED of the Hamiltonian, equation (1). The same procedure may be applied to many models involving particles with bosonic and/ or fermionic statistics.

　　ED is the straightforward way to obtain the eigenvalues and eigenvectors of a Hamiltonian. Naively, we first need the Hamiltonian written in matrix form in a particular basis of states. The apparent drawback is the fast growth of the dimension of this matrix, defined by the size of the basis, see table 1. In general, obtaining the full spectrum of the Hamiltonian, eigenvectors and eigenvalues, requires a number of operations which scales as $(\mathcal{N}_N^M)^3$. This makes the problem already intractable for fairly small quantum systems, and strictly impossible for larger ones.

　　Once the Hamiltonian matrix (or its action on arbitrary state vectors) is known, there are two classes of algorithms, direct and iterative methods, which can be used to completely or partially diagonalize a matrix, that is to find (at least) some of its eigenvalues and eigenvectors:

- *Direct methods* perform similarity transformations to the Hermitian (non-Hermitian) matrix of interest until it is written in a reduced form. Hermitian (general non-Hermitian) matrices are reduced to symmetric tridiagonal (upper Hessenberg) matrices. Once the matrix of interest is in the reduced form, it can be eigendecomposed in an efficient way with LU (QR) decomposition for Hermitian (non-Hermitian) matrices.

- In the *iterative projection methods*, the matrix operator is applied to a set of trial vectors, approximations to the eigenvalues are obtained from subspaces of lower dimension, and the iteration is continued until convergence is reached. Notice that they are able to approximate a number of eigenvalues and eigenvectors without any need to solve the entire system. Despite some of them are able to solve the entire system, it is not practical in most applications, due to a much larger number of operations than required by direct methods.

　　The direct methods are the only ones that are able to truly diagonalize a matrix, up to rounding machine errors, while the second ones obtain approximate partial solutions of increasing precision in an iterative way. On the other hand, direct methods require enough memory to store the full Hamiltonian and the similarity matrix, while iterative methods only need storage for a few state vectors. Matrix elements needed to compute the action of the matrix onto a state vector can either be determined on the fly, or stored in a less costly sparse-matrix format.

　　In our case, we have used an iteration projection method for sparse, Hermitian problems: the Lanczos algorithm. In order to implement it, a number of libraries are publicly available. Most of them only require a function which computes the action of the Hamiltonian on any given input vector, as explained below. It is important to know that there exist some preconditioners that transform the Hamiltonian, making it cheaper to evaluate or increasing the convergence for certain diagonalization methods,

such as the Jacobi–Davidson. An extensive and very pedagogical review about not only Hermitian problems, but numerical solving of algebraic eigenvalue problems can be found in [26].

3.1. Basis states and their ordering

In order to identify all the states of the basis, every state needs to have an associated label. The basis states should have a known and unique ordering, in order to be able to run loops over the vectors of the basis. Computing the action of the Hamiltonian on the vectors of the basis has to be as efficient as possible. In this work we have used the *Ponomarev* ordering [27]. It provides an efficient way to have all vectors of the basis labelled with a single integer ranging from 1 to the exact dimension of the Hilbert space, $\mathcal{N}_N^M$. In the procedure devised by Ponomarev, the mapping between a Fock state and its integer label can be carried out in both directions using a few, simple computational steps. It builds on a recursive relation for the dimensions of Hilbert spaces of different number of particles,

$$\mathcal{N}_N^M = \sum_{n=0}^{O} \mathcal{N}_{N-n}^{M-1} \quad \text{with } N, M, O > 0, \tag{17}$$

where O is the maximum occupancy per site, which sometimes is taken smaller than N to speed up the computations. Equation (17) allows one to devise a counting algorithm covering all numbers from 1 to $\mathcal{N}_N^M$. To perform the mapping, one first needs to evaluate all $\mathcal{N}_n^m$ occurring in equation (17).

　　Once this information has been obtained, the algorithm first re-writes the Fock state, determining the occupations of the M orbitals, into an N-component array $(m_1, m_2, \ldots, m_N)$, where m_i denotes the orbital in which the ith atom is. This becomes a simple one-to-one map by demanding $m_i \geqslant m_j$ for $i < j$. The integer label of the Fock state, n_β, is then obtained as

$$n_\beta = 1 + \sum_{j=1}^{N} \mathcal{N}_j^{M-m_j}. \tag{18}$$

　　With this, we can straightforwardly map a Fock state onto an integer label running from 1 to $\mathcal{N}_N^M$. The opposite map is slightly more complicated, as it involves an iterative procedure: given n_β, we find m_N by determining the largest $\mathcal{N}_N^m < n_\beta$. We then identify $m_N = m$, and continue to determine m_{N-1} by finding the largest $\mathcal{N}_{N-1}^m < n_\beta - \mathcal{N}_N^{m_N}$, and so on.

　　Let us see some examples. Consider for instance $N = M = O = 6$, with the $\mathcal{N}_n^m$ given in table 2, and the Fock vector $|\beta\rangle = |103020\rangle$. This tells us that the first site is occupied by one atom, the third site is occupied by three atoms, and the fifth site is occupied by two atoms. Accordingly, we re-write this information in agreement to the rule $m_i \geqslant m_j$ for $i < j$ as $(m_1, m_2, m_3, m_4, m_5, m_6) = (5, 5, 3, 3, 3, 1)$. Plugging this into equation (18), the integer label is then found as:

$$n_\beta = 1 + \mathcal{N}_1^1 + \mathcal{N}_2^1 + \mathcal{N}_3^3 + \mathcal{N}_4^3 + \mathcal{N}_5^3 + \mathcal{N}_6^5 = 258. \tag{19}$$

Table 2. Number of Fock states for a given N and M. The diagram shows the procedure to obtain the index for the Fock vector $|\beta\rangle = |211020\rangle$ for $N = 6$ and $M = 6$. The corresponding index is $n_\beta = 1 + 210 + 126 + 35 + 10 + 1 + 1 = 383$ out of the 462 states in the Hilbert space. The inverse procedure can also be read out, starting with $n_\beta = 383$, we look for the largest number in the $N = 6$ column which is already smaller than n_β, in this case, 210, we put one particle in the first mode, then we compare the remained with the values in the $N = 5$ column, turns out larger than 126, and so on. In the appendix we provide explicit Fortran codes for the procedures.

									n_{6-M}
	6	1	6	21	56	126	252	462	
	5	1	5	15	35	70	**126**	**210**	2
	4	1	4	10	20	**35**	56	84	1
M	3	1	3	6	**10**	15	21	28	1
	2	1	2	3	4	5	6	7	0
	1	1	**1**	**1**	1	1	1	1	2
	0	1	0	0	0	0	0	0	0
	0	0	1	2	3	4	5	6	
				N					

In table 2 we illustrate this mapping graphically for a second example, and explain how to operate in the inverse direction, that is from the integer label to the Fock state.

The inverse procedure, to go from the index to the actual Fock state is also fairly simple, subroutines coded in Fortran are provided in the appendix.

In our bosonic case, we have used the Fock states of populations of the lattice sites, see equation (2), allowing up to N particles per site and restricting the total number of particles in the system to N. For fermions the main difference is that the maximum population per site is 1, due to the Pauli exclusion principle, the labelling scheme works well simply considering $O = 1$ in equation (17).

3.2. Use of sparse matrices to store the Hamiltonian matrix

Since Hamiltonians are Hermitian, roughly half of the entries in the matrix are easily derived from the other half. This fact can be used to reduce storage memory, and to prevent us from redundant computations. Moreover, Hamiltonians of physical models are typically not very dense. In the case of the BHM, different states in the Fock basis are connected through hopping processes, but clearly this leads to non-zero matrix elements only between Fock states differing in two entries.

The most benefits of this sparseness can be made, if the matrix is stored in a sparse matrix format. We then only care about the non-zero elements which are stored in three 1D arrays of length L, with L being the number of non-zero elements. Typically, $\mathcal{N} < L \ll \mathcal{N}^2$, with $\mathcal{N}$ the Hilbert space dimension. Two of these arrays carry the integer labels of the pairs of states which are connected by the Hamiltonian (i.e. column and row of every non-zero matrix element). The third array stores the complex amplitude of such process, i.e. the value of the corresponding matrix element. In the case of the BHM, the length L is bounded from above by $(1 + Mz)\mathcal{N}_N^M$,

where z is the coordination number. Each Fock state can (at most) be connected to Mz other states through hopping processes, and to itself through the interaction.

3.3. Geometry of the lattice

In our computations we have considered a chain of atoms, but the topology and coordination number of the lattice could easily be changed. All information about the lattice is stored in an $M \times z$ array of adjacencies A. Its elements a_δ^i contain, for each site i, the labels δ of all neighbouring sites.

This can be extended to any kind of neighbourhood (nearest neighbours, next nearest neighbours, superlattices, anisotropic models, fully connected models,...). We then simply define a generalised array A of dimension $M \times z \times w$. Here, w counts the different types of neighbourhoods, and z is the largest coordination number in any neighbourhood. For instance, assume a 2D lattice with nearest- and next-nearest-neighbour hopping. Each site is then connected to 4 nearest neighbours, as well as 4 next-nearest neighbours, thus $z = 4$. We have two different types of connections, thus $w = 2$. Or consider a triangular lattice. In the isotropic case, each site is equally connected to six neighbours, e.g. $z = 6$ and $w = 1$. If the model becomes anisotropic, we have three types of connections, $w = 3$, to two different sites, $z = 2$.

The important advantage of implementing the lattice geometry as described here is its flexibility, specially in the implementation on inhomogeneous and anisotropic models. The counterpart, it should be said, is that it does not make use of lattice symmetries, like translational symmetry in the case of periodic boundaries, or parity symmetry for finite lattices. Since the Hamiltonian commutes with the corresponding symmetry operator, the Hamiltonian matrix is block-diagonal in the eigenbasis of a symmetry operator. The diagonalization can then be performed within each block separately. A comprehensive instruction for implementing translational symmetry in the ED code can be found in [22]. The largest block in the translationally invariant eigenbasis has a dimension which is approximately by a factor $1/M$ smaller than the full Hilbert space of N bosons on M sites.

3.4. Diagonalizing the Hamiltonian

As mentioned earlier, diagonalization algorithms differ greatly, but all of them need to calculate the action of the Hamiltonian onto the basis vectors. In exact methods the outcome of this calculation is stored in a matrix, and the unitary transformation diagonalizing this matrix is determined numerically. The advantage of the direct method is the fact that they provide the full spectrum of the Hamiltonian. However, direct methods are only feasible for matrix sizes on the order to $10^4 \times 10^4$, e.g. 7 particles in 10 sites, see table 1.

Beyond that, only iterative methods can be employed. Even where direct methods are still possible, iterative methods are much faster in providing only a few eigenvalues and eigenvectors. Iterative methods repeatedly apply the Hamiltonian on a set of state vectors, thereby filtering out an effective subspace. This procedure can be designed such that

the invariant subspace corresponds to the low-energy subspace. Since it is typically much smaller than the total Hilbert space, direct methods can finally be used to diagonalize the Hamiltonian within the low-energy subspace.

While the iterative methods do not require that the action of the Hamiltonian on a basis vector is stored in memory, nevertheless this information is frequently needed in order to perform the iterative multiplications. Thus, in particular if memory restrictions forbid to store this information, it is crucial for these algorithms to quickly evaluate the action of the Hamiltonian on a base vector 'on the fly'. For this goal, the labelling scheme presented above is an important ingredient.

Let us analyse the different steps the diagonalization algorithm has to go through. Consider an arbitrary state represented as a state vector in the Fock basis, $|\Phi\rangle = \sum_\beta^{\mathcal{N}_N^M} c_\beta |\beta\rangle$. The Hamiltonian is applied in two loops:

- One loop runs through all elements in the Fock basis, $i_\beta = 1, \ldots, \mathcal{N}_N^M$. In this loop, we perform a map from the state label i_β onto the occupation numbers.
- A second loop runs through all terms in the Hamiltonian, $\hat{H} = \sum_j \hat{H}_j$, where $\hat{H}_j$ is a monomial of creation and annihilation operators, e.g. $H_j = \hat{a}_3^\dagger \hat{a}_5^\dagger \hat{a}_2 \hat{a}_{14}$. Clearly, each step in this loop maps the state $|\beta\rangle$ onto a new basis state $|\beta'\rangle$, with an amplitude w_j^β:

$$\hat{H}_j |\beta\rangle = w_j^\beta |\beta'\rangle. \tag{20}$$

It is straightforward to determine both the new state $|\beta'\rangle$ in the occupation number basis, and the amplitude w_j^β. Using the mapping from occupation numbers onto state labels, we also find $i_{\beta'}$.

Accumulating the amplitudes w_j^β in the $i_{\beta'}$ th component of the new state vector, both loops together produce $|\Phi'\rangle = \hat{H}|\Phi\rangle$. In summary, the main computational task is the mapping between labels and states back and forth, and application of monomials to the states. Let us exemplify this for two of the monomials in equation (1). As an initial state we take the Fock state 383 from table 2, e.g. $|\Phi\rangle = \sum_i \Phi(i)|i\rangle = |383\rangle$, or $\Phi(i) = \delta_{i,383}$. First, we translate the Fock state into the occupation-number basis: $|\beta\rangle = |211020\rangle$. Then, we apply all monomials, e.g.

$$\frac{U}{2}\hat{n}_1(\hat{n}_1 - 1)|211020\rangle = \frac{U}{2}2 \times 1|211020\rangle$$
$$- t_{1,2}\hat{a}_2^\dagger \hat{a}_1|211020\rangle = = -2t_{1,2}|121020\rangle, \tag{21}$$

The first monomial corresponds to an interaction term. It is diagonal in the Fock basis and thus is easily evaluated. We accumulate on the output vector, $\Phi'(383) = \Phi'(383) + U\Phi(383)$. The second monomial represents a tunnelling term, and is not diagonal in the Fock basis, that is, it changes the state. The new state and the amplitude can easily be found, and using the Ponomarev mapping, we finally identify the label of the new state, $n_{121020} = 210 + 56 + 35 + 10 + 1 + 1 = 313$. This means, we accumulate the amplitude on that position the resulting vector, $\Phi'(313) = \Phi'(313) - 2t_{1,2}\Phi(383)$ in this case.

Once we have this procedure, the iterative methods will perform a number of calls to this procedure to obtain approximate values for the desired part of the spectrum. In this work we have used the ARPACK package [29], which requires on the order of 600 calls to this procedure to obtain the first 10 states of the Hamiltonian. With this, we are able to obtain the ground state and first excitations of systems of up to 5×10^6 states.

4. Results for the boundary between MI and SF

We are now ready to apply the ED method to the BHM. Our goal is to find the value of t/U at which the MI is no longer the GS of the system and it starts to be a SF in an infinite system with $N = M$, which is known as the critical value of the order parameter of the MI-SF transition at filling $q = 1$. Although we also show a few results for the 2D square lattice, our focus is on a homogeneous 1D Bose–Hubbard chain with nearest neighbour hopping. The SF to MI phase transition exhibited by the BHM with a commensurate number of particles, $N/M \in \mathbb{N}$, in d dimensions belongs to the $(d + 1)$D XY model universality class. For the 1D model, the exhibited phase transition is of the Berezinskii–Kosterlitz–Thouless type [1] (BKT). This phase transition is known to be infinite order—every derivative of the free energy is continuous—and very sensitive to finite size effects. As we will see in this section, this makes the determination the phase boundary extremely hard.

In order to interpret our numerical results, we will follow three different strategies: in section 4.1, we will consider the ground state vectors and determine their overlap with the analytic trial wave functions for the Mott phase and the SF phase. In section 4.2, we will analyse the insulating gap which in the thermodynamic limit closes at the transition point. In section 4.3, the scaling behaviour of the system is analysed. We shall stress that all three approaches come with their own limitations, which will be discussed in each subsection. Accordingly, it is also not surprising that each method produces quantitatively different results.

In all calculations, we restrict ourselves to hopping between neighbouring sites k and j, $t = t_{k,j}$. This keeps the essential symmetries to produce the MI to SF phase transition, see [28]. We also take $U = 1$, as only the ratio between t and U determines the system behaviour (for $U > 0$).

4.1. Overlap

Since we have the eigenstates of the system, which is a quantity that not every method is able to obtain, we may try to use this information to find the transition value. Then, we will compare the obtained ground states at different values of U/t with the analytical solution of the system in the cases $U/t = 0$ and $U/t = +\infty$. In particular, we compute the overlap between GS and trial states as a function of U/t,

$$\mathrm{OV} = |\langle \Phi_{\mathrm{Analytic}} | \Phi_{\mathrm{GS}} \rangle|. \tag{22}$$

J. Phys. B: At. Mol. Opt. Phys. **50** (2017) 113001

Tutorial
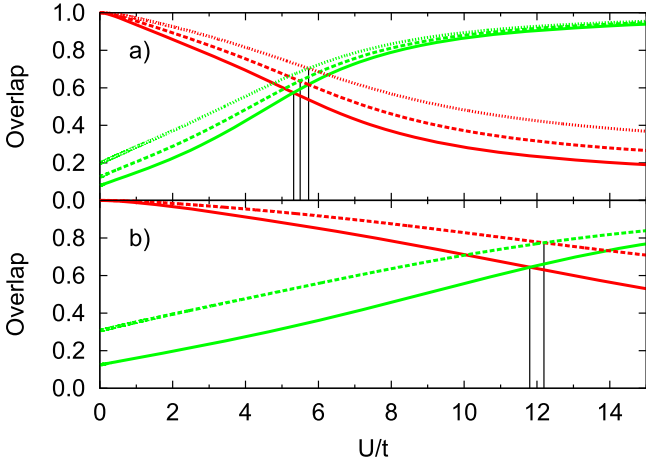
Figure 1. (a) Overlap of the GS of the system with the analytical SF (red) and MI (green) states in 1D lattices with periodic boundary of 5 (dotted line), 6 (dashed line) and 7 (solid line) sites. (b) Computations in 2D: 2×2 (dashed line) and 3×2 (solid line) lattices with periodic boundary. The abscissa where the two overlaps have the same value is marked to ease visualisation. Filling factor $q = 1$ so, $N = M$ in all the cases.

Figure 2. Finite-size scaling: the value of U/t at which the crossing of the overlaps happens is plotted as a function of $1/M$ for a 1D system with periodic boundary. The fitting to the analytical form, $U/t = a(M)^{-b} + c$ has been made with the non-linear least-squares Marquardt–Levenberg algorithm. This fit is used to extrapolate to the thermodynamic limit as explained in the text.

This overlap is never expected to be zero for finite systems, since the two trial states become orthogonal only in the thermodynamic limit. Analytically, we find

$$|\langle \Phi_{MI}(q)|\Phi_{SF}\rangle| = \sqrt{\frac{N!}{(M)^N (q!)^M}}. \qquad (23)$$

Therefore, this method is ill-conditioned for the BKT transition, but we show it for illustrative purposes. Nevertheless, the overlap OV can estimate the phase boundary by looking for the value U/t where both overlaps, for the MI and the SF phase, cross each other, that is, the GS of the system populates them equally, see figure 1. We denote this value by $(U/t)_N$, as it depends on the number of particles N. Performing a finite size study [30], we estimate the critical value in the thermodynamic limit, $(U/t)_\infty$, by extrapolation. We assume a size-dependency given by $\left(\frac{U}{t}\right)_M = AM^{-b} + \left(\frac{U}{t}\right)_\infty$, and perform the finite size study for the 1D systems.

This is a naive approach that is routinely used in the study finite-size effects of FQH systems. The size-dependency is chosen as a power with a variable exponent in place of a linear relation in order to capture any correction depending on non-integer powers.

The finite size study is shown in figure 2. The extrapolated value for the phase transition in the thermodynamic limit is $U/t = 4.45 \pm 0.04$, or, $t/U = 0.224 \pm 0.002$ with a reduced $\chi^2 = 6 \times 10^{-5}$. It is far indeed from most values in the literature, see [10] for an overview. The value found here lies between the one from third-order strong-coupling expansion [7] and the one from density-matrix renormalisation-group calculations [17].

Thus, based on our knowledge of overlaps in a small system, we are able to predict the phase diagram in the thermodynamic limit, although the overlap itself is certainly

not a good figure of merit for the BKT phase transition. In the following subsection, we take the opposite (and more systematic) approach, which characterises the phase boundary via an order parameter which, in the thermodynamic limit, vanishes exponentially in one of the phases.
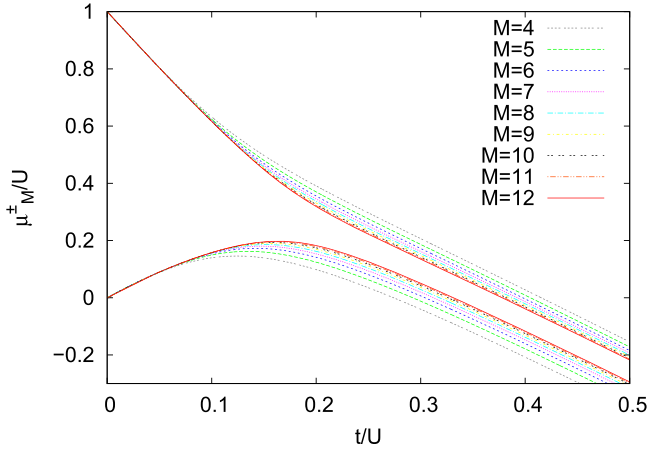
4.2. Insulating gap

By means of ED, we are able to find the ground state energy of the system with N particles in M sites at a given value of t/U, $E_0(t/U, M, N)$, in units of U, with machine precision.

According to [1], in the phase diagram of the BMH model, the critical value of the MI to SF phase transition is the value of t/U at which the upper and lower boundaries of each Mott lobe cross each other. We will try to exploit that idea defining an order parameter as the difference in ordinates between the two boundaries as function of t/U, following [31]. In the infinite system, that order parameter vanishes for the SF phase, as the boundaries cross each other at the transition value. Meanwhile, it remains finite as long as the GS of the system is the MI state. At first, we set a definition to find the upper and lower boundaries of the Mott lobes. According to [1], the upper (lower) boundary of a Mott lobe is given by exciton energy of one particle (hole) in the system. That is, the chemical potentials of the systems with M sites containing $M + 1$ ($M - 1$) particles. Then, we can find the upper (lower) boundary of the Mott lobe at filling q of the system of M sites, $\mu^+_{M,q}(t/U)$ ($\mu^-_{M,q}(t/U)$), as,

$$\mu^+_{M,q}(t/U) = E_0(t/U, M, qM + 1) - E_0(t/U, M, qM), \qquad (24)$$

$$\mu^-_{M,q}(t/U) = E_0(t/U, M, qM) - E_0(t/U, M, qM - 1). \qquad (25)$$

J. Phys. B: At. Mol. Opt. Phys. **50** (2017) 113001

Tutorial

Figure 3. Boundaries of the Mott insulator region with $N/M = 1$ for finite size systems. The sizes are $M = 4, 5, 6, 7, 8, 9, 10, 11, 12$. The upper family of curves is μ_M^+ and the lower is μ_M^-.

Figure 4. Single-particle excitation gap in the regime $q = 1$, for finite size systems. The sizes are $M = 4, 5, 6, 7, 8, 9, 10, 11, 12$.

In figure 3, the value of $\mu_{M,q=1}^+(t/U)$ and $\mu_{M,q=1}^-(t/U)$ is plotted as a function of t/U for $M = 4$ to $M = 12$. This figure shows the famous Mott lobes for finite systems. Notice that for our finite sizes and fixed number of particles, the boundary never closes, that is, the upper and the lower boundary of the lobe do not merge. However, it can clearly be seen how these two boundaries approach each other upon increasing the number of particles.

The energy gap in the MI phase, for any value of t/U, corresponds to the particle–hole excitation, which is the difference between $\mu_{M,q}^+(t/U)$ and $\mu_{M,q}^-(t/U)$ for a fixed t/U. So, we define the single-particle excitation gap of the lobe with filling q in a system with M sites as,

$$
\begin{aligned}
\Delta_{M,q}(t/U) &= \mu_{M,q}^+(t/U) - \mu_{M,q}^-(t/U) \\
&= E_0(t/U, M, qM + 1) + E_0(t/U, M, qM - 1) \\
&\quad - 2E_0(t/U, M, qM).
\end{aligned}
\tag{26}
$$

In the standard quantum phase transitions the single-particle excitation gap is particularly well suited as an order parameter because in an infinite system it vanishes in the SF phase, meanwhile it remains finite in the MI phase. Unfortunately, the single particle gap is not well suited to locate the transition in the iD case. In the BKT transition the gap is exponentially weak near the criticality, hardly detectable in finite systems. Hence, the formula above is by construction incorrect for small gaps in the MI phase. In addition, the studied systems exhibit finite size gaps due to the small size. Those gaps may dominate the single-particle excitation gap in the transition and clearly do in the SF phase, and besides, they can have different extrapolation exponents than the single-particle excitation gap. Obviously, a reliable extraction of the gap is also possible from Monte-Carlo methods, and possibly they will do a better job for this transition. The analysis of the energy gap performed in the present case, leads indeed to the results which do not have a clear physics meaning; nevertheless, one can estimate quite well the position of the criticality from that.
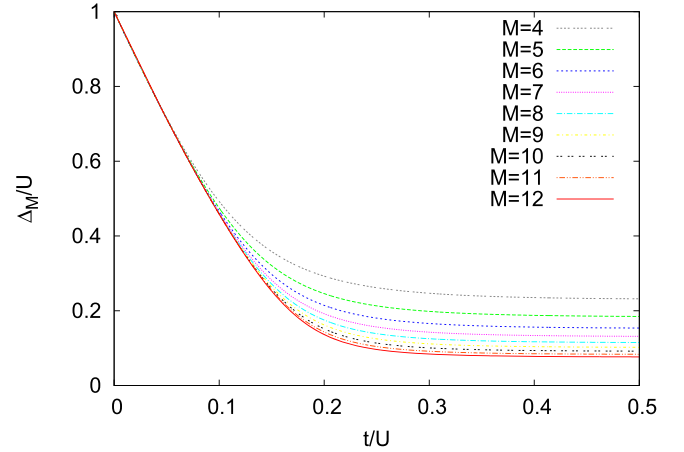
For simplicity, we define the single-particle excitation gap in the Mott lobe of filling 1 as $\Delta_M(t/U) \equiv \Delta_{M,q=1}(t/U)$. In figure 4, the value of $\Delta_M(t/U)$ is plotted as a function of t/U for M from $M = 4$ to $M = 12$. Notice that the gap does not vanish due to the mentioned domination of the finite size gaps in the SF phase, at large values of t/U, while the vanishing gap is an intrinsic property of the SF in the thermodynamic limit.

In order to determine the value of t/U for which the phase transition takes place, we have used values of $\Delta_M(t/U)$ as the plotted in figure 4 for M from $M = 3$ to $M = 13$. We have used here the fitting method from [31]: for every value of t/U, we fit $\Delta_M(t/U)$ to a fifth-degree polynomial of the inverse of the size, $1/M$. This expression has six fitting parameters. The constant term of the polynomial is $\Delta_\infty(t/U)$, which corresponds to the single-particle excitation gap of the thermodynamic system ($M \to \infty$) as function of t/U. Then, the phase transition takes place at the value of t/U for which $\Delta_\infty(t/U)$ just vanishes. The determination of $\Delta_\infty(t/U)$ through the regression is just a hidden extrapolation to the infinite system. Following [31], the behaviour of the extrapolation to $M \to \infty$ could imply a non-integer extrapolation exponent that a polynomial expression could not properly capture. In order to extrapolate the proper value of $\Delta_\infty(t/U)$ in the region where the finite size gaps could potentially play a role ($t/U \gtrsim 0.24$), we have used a fitting expression as function of $1/M^\alpha$ instead of $1/M$, where α is a positive real exponent. This adds one extra free parameter to the fitting expression.

The obtained values of $\Delta_\infty(t/U)$ as function of t/U for three sets of sizes $M \in \{3, \ldots, 13\}$, $M \in \{4, \ldots, 13\}$ and $M \in \{5, \ldots, 13\}$ are shown in figure 5, along with the corresponding value of the exponent α. The log scale has been used for an easier visualisation of the vanishing point. In figure 5, the behaviour of $\Delta_\infty(t/U)$ in units of U is roughly similar for every set of sizes: it starts at 1 for $t/U = 0$ and monotonically decreases to 0 at $t/U \approx 0.285$. For $t/U \gtrsim 0.285$, the different sets show different behaviours: The set with sizes $M \in \{3, \ldots, 13\}$ shows negative, small values of $\Delta_\infty(t/U)$, while the set with sizes $M \in \{5, \ldots, 13\}$ shows even smaller,

J. Phys. B: At. Mol. Opt. Phys. **50** (2017) 113001

Tutorial
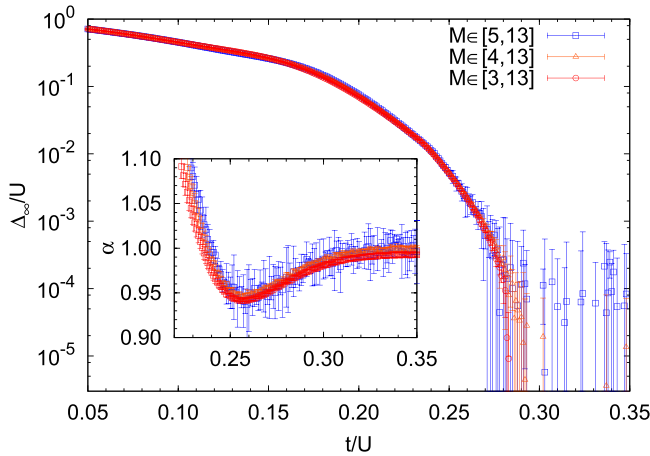
Figure 5. Extrapolated value Δ_∞ as a function of t/U in a log scale for three different sets of sizes. The inset shows the value of the fitting parameter α as a function of t/U for each set of data. The errorbars show the 95% confidence intervals.

positive and negative values, whose errorbars make them mainly compatible with 0. The set with sizes $M \in \{4,...,13\}$ shows an intermediate behaviour. It shows positive and negative values of $\Delta_\infty(t/U)$, that are smaller in magnitude than in the former set, but they are more biased to negative values than in the latter set. Some of the values are incompatible with 0. Obviously, any value $\Delta_\infty(t/U) < 0$ is clearly unphysical. Still, the value of $\Delta_\infty(t/U)$ and its dependence on t/U suggest that are a reasonable way to identify the criticality. The value of $\Delta_\infty(t/U)$ deep in the SF phase is not zero as we know it should, but a negative small value. This is because we did an extrapolation from small, finite sizes that led to an inaccurate values of the y-intercept, $\Delta_\infty(t/U)$. As we restrict the analysis to sets of larger sizes, the value of $\Delta_\infty(t/U \to \infty)$ goes closer to zero, becoming less negative, and even erratic around zero. Consequently, we will treat any small negative value as what it is: an unphysical value that has been obtained just because it is the one that better meets the fitting relation with data from small systems. So, the estimation of the critical value $(t/U)_c$ will be the value of t/U for which Δ_∞ crosses zero for first time and its uncertainty will be the difference between the latter value and the value of t/U at which the errorbar has crossed zero for first time. Then, the obtained critical value for the sets $M \in \{3,...,13\}$, $M \in \{4,...,13\}$, and $M \in \{5,...,13\}$ using this method is $(t/U)_c = 0.285 \pm 0.002$, $(t/U)_c = 0.292 \pm 0.006$, and $(t/U)_c = 0.283 \pm 0.009$ respectively. Being conservative, we estimate the critical value with this method as the mean of the latter values, weighted with the relative error, giving $(t/U)_c = 0.286 \pm 0.017$. Notice that the set of bigger sizes has 8 different sizes and its data is fitted with an expression with up to 7 free parameters. The fact that this system is minimally overdetermined leads to some instability in the values of the fitting parameters and to bigger uncertainties.

The fitting parameter α has remained within the range [0.94, 1.00] for all the values of t/U used in the analysis. Notice that the transition value of the [31], $(t/U)_c = 0.275 \pm 0.005$, is compatible with ours. Interestingly enough, our values of the fitting parameter α near the transition are also compatible with

their value $\alpha = 0.95$. Also notice the strong discrepancy with the estimation from the previous naiver method. Despite this method is nothing more than an elaborated extrapolation to infinite size, the final result with this method is within the range of the most recent studies. It is also compatible with most of values in the literature, due to its broad uncertainty margins.

4.3. Finite-size effects of the gap

We may try to focus in a more general procedure in order to try to get rid of the finite size effects. The way to proceed in most of phase transitions is the general finite-size scaling hypothesis. According to it, close to the phase transition, and with the proper finite-size power rescaling of the order and control parameters, the curves for different sizes should collapse into a single curve, independent of the size of the system, called universal scaling function. In our case, order and control parameters would be $\Delta_{M,q}$ and t/U, respectively. Regrettably, the exponential closing of the gap characteristic of the BKT transition does not allow such development. Since the gap in the SF phase closes as $\Delta \sim \exp\left[-\frac{g}{\sqrt{|(t/U)_c - t/U|}}\right]$ —with g being an unknown constant—the finite-size corrections become logarithmically small, not potentially as the finite-size scaling hypothesis assumes and therefore, the finite-size power rescaling is not suitable. As a consequence of this behaviour, the BKT transition is known to converge to the thermodynamic limit very slowly when increasing the size of the system. This is, in order to get rid of finite size effects, order parameter curves corresponding to sizes from a wide range of orders of magnitude are essential.

We have followed an approach similar to the one of the authors of [14, 32]. They propose an ansatz for the scaling relation of the single-particle excitation gap, $\Delta'_{M,q}(t/U) = M\Delta_{M,q}(t/U)\left[1 + \frac{1}{2\ln(M) + C}\right]$ where $\Delta'_{M,q}(t/U)$ is the rescaled gap, and C is an unknown constant. Those authors found that $C \to \infty$ for the standard BHM so, the logarithmic correction becomes negligible. We defined the rescaled reduced control parameter as $\tilde{t} \equiv \frac{t/U - (t/U)_c}{(t/U)_c}M^a$, where a is an scaling exponent. The former takes the value $\tilde{t}_c = 0$ at criticality. We also propose the rescaling $\Delta'_M \equiv \Delta_M M^b$ for the order parameter, where b is an scaling exponent. Both, a and b are related to the critical exponents of the universality class of the phase transition. From it we already knew that they should be $a = 1/2$ and $b = 1$, respectively. Notice that this implies a potential relation that will deviate from the one given by [14] for large enough systems. Although ED does not allow to compute large enough systems to obtain finite-size effect free results, we proceed with the analysis of the obtained results for illustrative purposes.

We use the fact that, at criticality, the order parameter collapses in a single size-independent universal curve to find the proper exponents and the critical value of the phase transition through a minimisation of the squared differences between curves of different sizes. Far from the phase transition, the subleading therms overcome the scaling relation and then, the rescaled order parameter depends on the size of the

J. Phys. B: At. Mol. Opt. Phys. **50** (2017) 113001

Tutorial

system. The problem is to determine how far from the phase transition the system starts to exhibit resolvable finite size effects, and so, which interval of data points has to be taken in consideration for the minimisation. We call $\tilde{t}^-$ ($\tilde{t}^+$) the lower (upper) limit of that interval. That is, the curves of the rescaled order parameter follow the same curve in the interval $[\tilde{t}^-, \tilde{t}^+]$ around the criticality. Then, we define the figure of merit of the minimisation as,

$$S((t/U)_c, a, b) = \sum_{M > M'} \int_{\tilde{t}^-}^{\tilde{t}^+} \Delta'_M(\tilde{t}) - \Delta'_{M'}(\tilde{t}) \mathrm{d}\tilde{t}, \quad (27)$$

where the integral is calculated numerically over interpolation of the data points with cubic splines.

Since we do not know how far from the critical point the system starts to exhibit resolvable finite size effects, we try to collapse the curves for several system sizes M as function of $\tilde{t}^-$ and $\tilde{t}^+$ with the following procedure:

- For a given value of $\tilde{t}^-$, we fix $\tilde{t}^+ = -\tilde{t}^-/e$, since we have visually realised that the lowest values of S are achieved when $\tilde{t}^+ \sim -\tilde{t}^-/2$ holds.
- We minimise S changing the set of parameters $((t/U)_c, a, b)$.

Then, we find an optimum set of parameters $((t/U)_c, a, b)$ as a function of $\tilde{t}^-$. We may expect that when $\tilde{t}^-$ is very small, the number of data points is not enough to properly describe the universal scaling function, due to the lack of resolution. On the other side, when $\tilde{t}^-$ is large enough, the finite size effects play a role and the curves are no longer collapsed in the universal scaling function. This leads to obtaining parameters that are size-dependant and not related to the universal scaling function.

For a range of $\tilde{t}^-$ in between, we may expect to have a constant, size-independent values of the parameters, showing a plateau. This is due to the fact that the curves are collapsed in a universal scaling function, which has the same parameters for any choice of $\tilde{t}^-$ and sizes M. In order to control those possible size dependency of the parameters $((t/U)_c, a, b)$, we have computed those parameters taking in account different sets of curves: pairs of consecutive sizes ($M = 11$ and 12, 9 and 10, 7 and 8,...), subsets of the larger systems (from $M = 9$ to 12, from 8 to 12,...) and for all of them.

The parameters $(t/U)_c$, a, and b for a several size sets are shown in figure 6. According to those results, the estimated values are: $(t/U)_c = 0.3115 \pm 0.0010$, $a = 0.5010 \pm 0.0010$, and $b = 0.9870 \pm 0.0010$. The fact that the parameters that we have found do not have a resolvable size dependency seems quite noticeable. It is because our set of sizes are too clustered to resolve the differences due to the size. Notice that we have let both exponents, a and b, to vary, despite we know their value. This allows to explore a broader area of the space of parameters to improve the final value of $(t/U)_c$, and let the minimisation find the proper scaling exponents by itself. Additionally, it gives us a proof of the goodness of the scaling. As a matter of fact, the value of the exponent b is several error bars below the expected value $b = 1$. It is due to the fact that the small sizes we studied did not allowed to get rid of the finite-size effects. Then, the
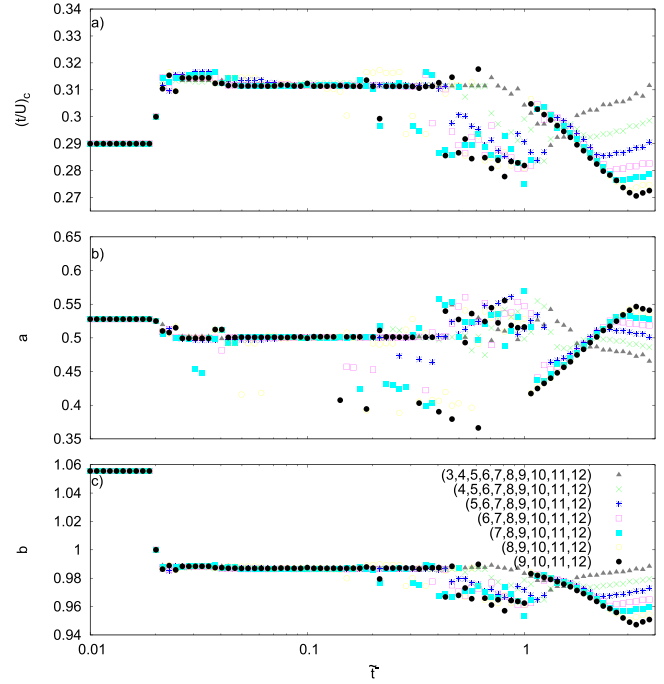
Figure 6. Optimal values of $(t/U)_c$, a and b as a function of $\tilde{t}^-$ to collapse several sets of system sizes M.

analysis has led to a non-universal coefficient. Reminding that the size corrections in the BKT transition are logarithmic becomes clearer that the set of sizes shall include sizes with larger orders of magnitude. It has to be stated that potential scaling relations are wrong for analysing the BKT transition, but with this treatment a good value is fortuitously obtained because of the small sizes studied—given that the value obtained for the exponent b does not correspond to the expected, 1. Finally, the collapse of various system sizes with those parameters is shown in figure 7.

4.4. Summary

Given that the most recent numerical results localise the BKT transition at values t/U between 0.26 and 0.31, we must clearly state that our first approach considering the overlaps fails, as it yields $(t/U)_{\mathrm{crit}} = 0.224 \pm 0.002$. Despite the nature of the BKT and the weakness of the gap even in the insulating phase, the second method produces a result which agrees with the literature, $(t/U)_{\mathrm{crit}} = 0.286 \pm 0.017$. Also our third approach, the scaling analysis, produces a result which is still compatible with the literature, 0.3115 ± 0.0010, although the underlying scaling hypothesis does not hold for the BKT transition.

5. Beyond the standard BHM

A number of modifications to the standard BHM have been studied. Those modifications include different topologies and coordination numbers of the lattice, inhomogeneous potentials, negative interactions, additional neighbouring interactions, long
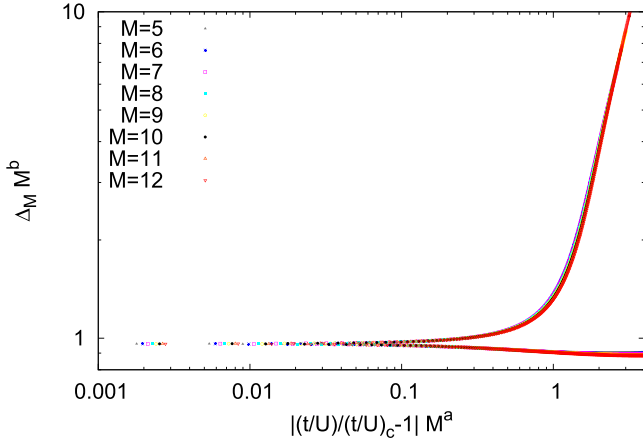
Figure 7. Collapse of the curves for $M = 5, 6, 7, 8, 9, 10, 11,$ and 12 sites for the estimated parameters $(t/U)_c = 0.3115$, $a = 0.501$, and $b = 0.987$ in a log–log scale.

range interactions, among others. ED very suitable for most of those modifications, due to the lack of assumptions on the parameters. We have played with a couple of modifications: inhomogeneous lattices, and attractive on-site interactions.

5.1. Phase transitions in a deeply biased lattice

An interesting modification of the SF to MI transition is obtained by considering a lattice with a large attractive bias. In this case the tendency to form a SF is suppressed, as in the limit of weak interactions the particles prefer to localise on the biased site. Increasing repulsive interactions, the system reaches the Mott phase, undergoing several transitions in which the number of particles on the biased site is reduced by one. The large inhomogeneity is produced by making the potential energy in the kth site much lower than the others. Theoretically, we take it into account by adding the term $-\epsilon \sum_i^M \hat{n}_i \delta_{i,k}$ to the Bose–Hubbard Hamiltonian.

To evaluate the effect of the bias potential in the system, we introduce the fluctuation of the number operator in the ith place,

$$(\Delta \hat{n}_i)^2 = \langle (\hat{a}_i^\dagger \hat{a}_i)^2 \rangle - \langle \hat{a}_i^\dagger \hat{a}_i \rangle^2. \tag{28}$$

It can be written explicitly with the number operators in the Fock basis. Moreover, due to the fact that the Fock states are eigenstates of $\hat{n}_i$, the only nonzero contribution occurs when $|\beta'\rangle = |\beta\rangle$. So,

$$(\Delta \hat{n}_i)^2 = \sum_\beta |c_\beta|^2 \langle \hat{n}_{i\beta^2} \rangle - \left[\sum_\beta |c_\beta|^2 \langle \hat{n}_{i\beta} \rangle \right]^2, \tag{29}$$

where $\langle \hat{n}_{i\beta} \rangle$ means $\langle \beta \hat{n}_i | \beta \rangle$. The fluctuation of the on-site number of particles may serve as a precursor of a phase transition which involves redistribution of the particles in the ground states. In the presence of a strong bias potential, $\epsilon \gg t$, several peaks of the number fluctuations occur upon tuning U/t.

In figure 8, we chose $\epsilon = 100t$, and study a square lattice consisting of a single plaquette, that is, four sites. Accordingly, we observe $N - 1 = 3$ peaks of the number fluctuations upon
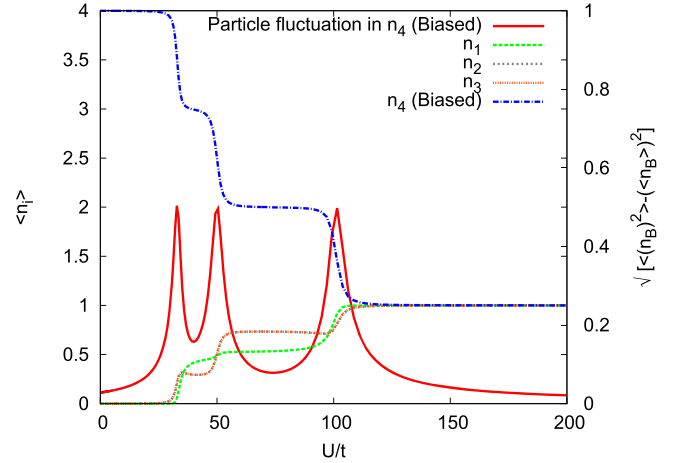
Figure 8. Transition from the fully localised state to the MI phase in a deep biased 2×2 lattice with open boundary condition. The bias is taken to be $\epsilon = 100t$ in the 4th site. The values of the average population of all sites is depicted together with the fluctuation of the number of particles in the biased site (red solid curve). The direct hopping between the 4th site and the 1st is not allowed and hopping between the 4th and the 2nd and 3rd are equivalent. Note the clear peaks in the number fluctuation for fixed values of U/t corresponding to the transitions described in the text.

tuning from $U/t = 0$ to large values of U/t. In order to infer which mechanisms produces the fluctuations, we have calculated the population of each site in the lattice, simply by taking the diagonal values of the OBDM, plotted in figure 8. When the fluctuation reaches a maximum, the population in the biased site decreases by one. Between two consecutive fluctuation peaks, the populations remain mainly constant, showing plateaus with a step structure. The last peak of the fluctuations, occurring at the largest value of U/t, indicates a transition into the MI phase: we find that for larger values of U/t, the population of all the sites takes the same integer value q, and the fluctuation decrease monotonically to zero.

The values of U/t for which fluctuation maxima appear can be parametrised by $U/t = 100/i$, for $i = 1, \cdots, N - 1$. These values are easily explainable for the MI with $q = 1$, keeping in mind the Hamiltonian in equation (1): the migration happens when the energy of keeping the particles in the same site becomes greater than extracting one particle from the biased site to place it in other site without particles,

$$\frac{U}{2} n_B (n_B - 1) - \epsilon n_B = \frac{U}{2} (n_B - 1)(n_B - 2) - \epsilon (n_B - 1), \tag{30}$$

where we have neglected the hopping term t, which is small compared to ϵ and U. The subindex B denotes the biased site. From this equation, we obtain the condition,

$$U = \frac{\epsilon}{n_B - 1}, \tag{31}$$

where n_B is a positive integer which $1 < n_B \leqslant N$.

As can be seen in figure 8, in general the unbiased sites are not equally populated. When the interaction is large enough to expel the first particle from the biased site, the second most populated site is the one which is not directly

J. Phys. B: At. Mol. Opt. Phys. **50** (2017) 113001

Tutorial

connected to the biased site. This might appear counter-intuitive in the first place, but one has to bear in mind that a particle on this site benefits from having two empty neighbours, allowing to reduce energy by tunnelling processes to these sites. On the other hand, once a second particle is pushed out from the biased site, the situation changes, and two nearest neighbours of the biased site become more populated. But now, two particles occupying these two sites still can share the empty neighbouring site for virtual tunnelling.

5.2. Attractive interactions: localisation

As studied for the two-site case in [20, 21], systems with attractive interactions feature large quantum superpositions due to the several competing single-particle ground states [25].

For $U/t = -\infty$, all the particles in the system will aggregate in a single site, so the GS is the Fock state with N particles in the ith site and 0 in the other sites. But this state is M-degenerate. Due to this degeneracy, the ground state can be a superposition of these M states. Each one of them aggregates the system in one different site of the lattice. In this state, when a particle is fixed in one site, all the rest cluster there. So, this state is highly correlated. For the two site case, the ground state build a so-called NOON state [20].

In any practical implementation there will be small imperfections that will trigger small biases between the sites. It is thus expected, that for sufficiently large attractive interactions in realistic systems, the GS will be unique with all particles clustered in one site. To account for such effects, we consider a slightly biased case which favours one site, the kth.

The localised condensate (LC) state in the kth site of the lattice, reads,

$$|\Psi_{\mathrm{LC}}(k)\rangle = \frac{1}{\sqrt{N!}}(\hat{a}_k^\dagger)^N |0\rangle. \tag{32}$$

In this state, as in the MI, the number of particles in each site is well defined and the correlation length vanishes. Different from the MI, also the energy gap vanishes, and its value is given by the value of the bias. Since this state is a single state of the Fock basis with all the particles localised in the same site, the values of S_1 and S_D are both 0.

It is noticed that if several sites on the lattice were biased significantly more than the rest, it could be possible to obtain a fragmented condensate. It is also possible to engineer the number of fragmented fractions by setting a number of biased sites in the lattice.

To understand the system behaviour for intermediate values of the attractive interactions, we apply ED and calculate the entropy S_D as function of NU/t. The results are depicted in figure 9. The entropy has its maximum in the attractive regime, not at $U/t = 0$ where the entropy S_1 exhibits a minimum. This observation implies that the GS of a weakly attractive system is more uniformly distributed over the Fock basis than the GS of the SF phase. Increasing the attractive interaction, but keeping the bias smaller than the gap, the system is in a cat-like state, with $S_D = \ln(M)$. By
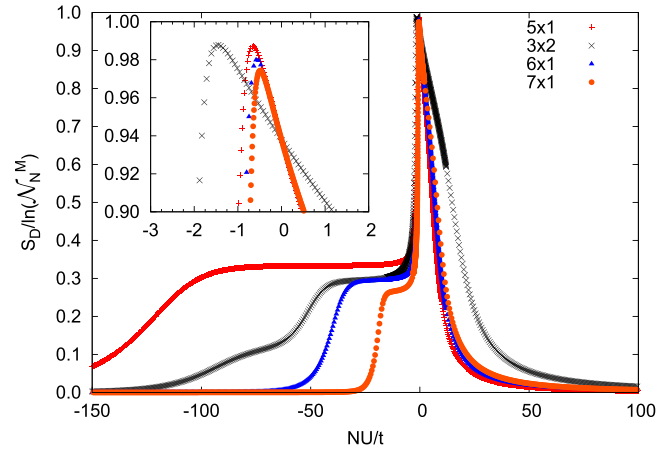
Figure 9. Entropy S_D of the GS in a system with attractive interactions, for 5–7 particles in different geometries with periodic boundaries. The plot is zoomed in order to appreciate the weakly attractive regime. In particular, it is worth emphasising the fact that the maximum of the entropy, maximal delocalisation in Fock space, is not achieved for zero interaction but for slightly attractive one. The bias is $\epsilon = 10^{-10} t$.

cat-like state we mean a superposition state of events that mutually exclude each other from happening simultaneously, in this case, the superposition of clustering all the particles in every site of lattice. Finally, for even stronger attraction, the gap becomes smaller than the bias. Then the bias term dominates and the system localises on a single site, with a single Fock state being the ground state.

The phenomenon is similar to the one studied in [21]. There, the system is found to go from a binomial distribution in Fock space, to a very homogeneous one at slightly attractive interactions. Further increasing the interactions, the distribution does not become more homogeneous, but instead starts to develop peaks around each of the two-sites, which corresponds to the two superposed states of the cat-like structure. In presence of a small bias, further increasing the attractive interaction, the system localises.

Effects in the weakly attractive regime in higher dimensions than 1D are finite-size effects, since in the thermodynamic limit, a soft-core system of bosons collapses at any finite value of attractive interactions [33]. In 1D, due to the interplay between the kinetic energy and the attractive interaction energy, bright soliton solutions arise from the Gross–Pitaevskii equation [34].

Notice that in the weakly attractive regime, the number of populated Fock states increases when interactions are strengthened, but the distribution becomes less uniform. This behaviour is more pronounced in the cases with open rather than periodic boundary conditions, as open boundary provide a natural bias with less connected sites at the edge of the system.

5.3. ED for other problems: quantum Hall physics

When it comes to studying BHMs with ED, the reader has to notice that, despite its insurmountable size limitations, one strength of the method is its applicability to a wide

J. Phys. B: At. Mol. Opt. Phys. **50** (2017) 113001

Tutorial

range of problems. As example, just adding complex values to the tunnelling, models with gauge potentials can be studied.

In this section, we will briefly outline how the method can also be applied to continuum systems. As an example, we choose the fractional quantum Hall effect, which can be exhibited by fermionic particles (electrons), but also by bosons, e.g. a cold gas of bosonic atoms rotating around the z axis in 2D [35]. In this bosonic scenario, we shall find some analogies to the treatment of the BHM.

The first step for treating the problem by ED again is to construct a basis for the Hilbert space. In the quantum Hall effect, the single-particle energy levels are the Landau levels (LLs), and it is usually enough to consider only one LL, for bosons the lowest LL (LLL). All states in the LLL are degenerate, and can be labelled by a quantum number $l \geqslant 0$, the angular momentum along the rotation axis. These angular momentum eigenstates play a role analogous to the sites in the BHM, and it allows to map between the basis for the BHM onto the basis of bosons in the LLL. Since, in principle, there are infinitely many single-particle states, though, we have to truncate the basis at a sufficiently large $l = l_{max}$. Due to rotational symmetry, the total angular momentum L along z is conserved. This provides a natural value $l_{max} = L$ for truncating the Hilbert space, but in practice the available angular momentum will be distributed more equally between all particles, so l_{max} can be chosen much smaller, at the order $l_{max} \sim L/N$ for N bosons.

In contrast to the BHM, due to the degeneracy of single particle levels in the fractional quantum Hall problem, there is no single-particle term in the Hamiltonian. Taking into account a trapping potential only introduces a L-dependent energy shift. The interactions, though, are much more difficult to treat than in the BHM, as two particles at l and l' may scatter to arbitrary orbitals $(l + l')/2 + x$ and $(l + l')/2 - x$. The interactions may lift the huge single-particle degeneracy, and may give rise to a unique state describing a fractional quantum Hall phase. In order to interpret the numerical results, one tries to identify the fractional quantum Hall phases by scanning through different values of L, searching for pronounced gaps. Similar to our strategy presented in section 4.1, one can then compare the numerical ground state with trial wave functions by evaluating their overlaps.

In practical applications, the number of particles is clearly restricted to a small numbers, $N \lesssim 20$. The studies of mixtures of multicomponent systems restricts the computations to even smaller numbers. For those systems, a subspace containing every Fock–Darwin state of every species [36] is constructed. The total Hilbert space is direct sum of the subspaces, and hence, the total dimension of the space is the product of dimensions of those subspaces.

6. Conclusions

We have provided a comprehensive study of BHMs composed of a small number of atoms, $\simeq 10$ populating a small number of sites, $\simeq 10$. First, we have introduced the BHM together with a detailed description of the ED technique employed. Then we have concentrated in the MI to SF transition, first discussing its characterisation by means of exact overlaps with trial wave functions and secondly by performing finite size scaling of the gap.

We have also studied a highly biased lattice, in which one site is considerably deeper than the others. In this case, the system undergoes several transitions, from a fully localised state to a MI phase, going through partial SF phases, in which more and more atoms delocalised prior to localising in the MI. The way the MI phase grows in population has been shown to proceed stepwise as the interaction is increased.

In the attractive interactions case, we have considered a small biased case, to understand the competition between attraction and localisation. For sufficiently large attractive interactions, the system fully localises due to the bias. At lower attractions, the system develops a cat like structure. Prior to this, the system goes through a state in which the number of populated Fock states is maximal.

Acknowledgments

Appendix. Subroutines for the labelling procedure

Explicit Fortran subroutines to generate the Fock basis labelling as explained in section 3.1. First we need to build the Pascal triangle, depending on the total number of sites and particles, this is done with **buildpascal**. Once this is generated, we can use **b2in** and **in2b**, to from the basis to the index or vice versa, respectively.

```
c original from A. V. Ponomarev (2009)
   subroutine buildpascal
c lc = number of sites +1
c nc = number of atoms +1
   parameter (lc = 4, nc = 3)
   double precision jbc
   integer cnkc(lc,nc)
   integer jmax
   common/pascal/jmax,cnkc
c builds the rotated pascal triangle
   do i = 1, lc
     cnkc(i,1) = 1
   end do
   do i = 1, lc
```

<div style="text-align:center">(Continued.)</div>

```
  do j = 2,nc
    cnkc(i,j) = 0
  end do
 end do
 do in1 = 2,lc
 cnkc(in1,2) = sum(cnkc(in1-1,1:2))
 if (nc-1.gt.1) then
 do in2 = 1,nc
  cnkc(in1,in2) = sum(cnkc(in1-1,1:in2))
 end do
 end if
 end do
 jmax = cnkc(lc,nc)
 end
```

```
c———————————————————————————
c Returns the many body state bi at position in
c———————————————————————————
c original from A. V. Ponomarev (2009)
  subroutine b2in(bi,in)
  implicit none
  integer in,lc,nc,jmax,ind_L,ind_N,indi,k,
 is,i
  parameter (lc = 4,nc = 3)
  integer cnkc(lc,nc),bi(lc),suma,M,in1,in2
  common/pascal/jmax,cnkc
c builds the rotated pascal triangle
  in = 1
  do indi = 1,lc-2
  do ind_N = 0,bi(indi)
  if (bi(indi)-ind_N.gt.0) then
    suma = 0.
    do k = 1,indi-1
    suma = suma+bi(k)
    enddo
  if (lc-indi.gt.0.and.nc-ind_N-suma.
 gt.0) then
    is = 0
   in = in+cnkc(lc-indi,nc-ind_N-suma)
  endif
  endif
  enddo
  enddo
  end
```

```
c———————————————————————————
c Returns the many body state bi at position in
c———————————————————————————
c original from A. V. Ponomarev (2009)
  subroutine in2b(in,bi)
  implicit none
  integer in,lc,nc,jmax,ind_L,ind_N,indi
  parameter (lc = 4,nc = 3)
  integer cnkc(lc,nc),bi(lc)
  common/pascal/jmax,cnkc
   indi = in-1
   bi = 0
   ind_L = lc-1
```

<div style="text-align:center">(Continued.)</div>

```
  ind_N = nc
  do while(ind_N.ne.1)
   if(indi.ge.cnkc(ind_L,ind_N)) then
    indi = indi-cnkc(ind_L,ind_N)
    bi(lc-ind_L) = bi(lc-ind_L)+1
    ind_N = ind_N-1
   else
    ind_L = ind_L-1
   end if
  end do
 end
```

References

[1] Fisher M P A, Weichman P B, Grinstein G and Fisher D S 1989 *Phys. Rev.* B **40** 546–70

[2] Lewenstein M, Sanpera A and Ahufinger V 2012 *Ultracold Atoms in Optical Lattices: Simulating Quantum Many-body Systems* (Oxford: Oxford University Press) (https://doi.org/10.1093/acprof:oso/9780199573127.001.0001)

[3] Greiner M, Mandel O, Esslinger T, Hansch T W and Bloch I 2002 *Nature* **415** 39–44

[4] Buonsante P and Vezzani A 2007 *Phys. Rev. Lett.* **98** 110601

[5] van Oosten D, van der Straten P and Stoof H T C 2001 *Phys. Rev.* A **63** 053601

[6] Gelfand M, Singh R and Huse D 1990 *J. Stat. Phys.* **59** 1093–142

[7] Freericks J K and Monien H 1996 *Phys. Rev.* B **53** 2691–700

[8] Rokhsar D S and Kotliar B G 1991 *Phys. Rev.* B **44** 10328–32

[9] Jaksch D, Bruder C, Cirac J I, Gardiner C W and Zoller P 1998 *Phys. Rev. Lett.* **81** 3108–11

[10] dos Santos F E A and Pelster A 2009 *Phys. Rev.* A **79** 013614

[11] Teichmann N, Hinrichs D, Holthaus M and Eckardt A 2009 *Phys. Rev.* B **79** 224515

[12] Graß T D, dos Santos F E A and Pelster A 2011 *Phys. Rev.* A **84** 013613

[13] Schollwöck U 2005 *Rev. Mod. Phys.* **77** 259–315

[14] Carrasquilla J, Manmana S R and Rigol M 2013 *Phys. Rev.* A **87** 043606

[15] Prokof'ev N, Svistunov B and Tupitsyn I 1998 *Phys. Lett.* A **238** 253–7

[16] Cazalilla M A, Citro R, Giamarchi T, Orignac E and Rigol M 2011 *Rev. Mod. Phys.* **83** 1405–66

[17] Batrouni G G, Scalettar R T and Zimanyi G T 1990 *Phys. Rev. Lett.* **65** 1765–8

[18] Batrouni G G and Scalettar R T 1992 *Phys. Rev.* B **46** 9051–62

[19] Kashurnikov V, Krasavin A and Svistunov B 1996 *J. Exp. Theor. Phys. Lett.* **64** 99–104

[20] Cirac J I, Lewenstein M, Mølmer K and Zoller P 1998 *Phys. Rev.* A **57** 1208–18

[21] Juliá-Díaz B, Dagnino D, Lewenstein M, Martorell J and Polls A 2010 *Phys. Rev.* A **81** 023615

[22] Zhang J M and Dong R X 2010 *Eur. J. Phys.* **31** 591

[23] Penrose O and Onsager L 1956 *Phys. Rev.* **104** 576–84

[24] Penrose O 1951 *Phil. Mag. Ser.* 7 **42** 1373–7

[25] Mueller E J, Ho T L, Ueda M and Baym G 2006 *Phys. Rev.* A **74** 033612

[26] Bai Z, Demmel J W, Dongarra J J, Ruhe A and Van Der Vorst H A (ed) 2000 *Templates for the Solution of Algebraic Eigenvalue Problems: A Practical Guide* (*Software, Environments, Tools*) (Philadelphia, PA: SIAM) (https://doi.org/10.1137/1.9780898719581)

[27] Ponomarev A V 2009 Private communication
　　 Ponomarev A V, Denisov S and Hänggi P 2011 *Phys. Rev. Lett.* **106** 010405
　　 Ponomarev A V, Denisov S and Hänggi P 2010 *Phys. Rev. A* **81** 043615
　　 Ponomarev A V, Denisov S and Hänggi P 2009 *Phys. Rev. Lett.* **102** 230601
[28] Rey A M 2004 *Ph. D. Thesis* University of Maryland
[29] Lehoucq R, Sorensen D and Yang C 1997 *Arpack Users' Guide: Solution of Large Scale Eigenvalue Problems with Implicitly Restarted Arnoldi Methods* (Philadelphia, PA: SIAM)
[30] Campostrini M and Vicari E 2010 *Phys. Rev. A* **81** 023606

[31] Elesin V F, Kashurnikov V A and Openov L A 1994 *Pis'ma Zh. Eksp. Teor. Fiz.* **60** 174
　　 Elesin V F, Kashurnikov V A and Openov L A 1994 *J. Exp. Theor. Phys. Lett.* **60** 177
[32] Mishra T, Carrasquilla J and Rigol M 2011 *Phys. Rev. B* **84** 115135
[33] Abdullaev F K and Garnier J 2008 *Bright Solitons in Bose–Einstein Condensates: Theory* (Berlin: Springer) pp 25–43
[34] Gordon J P 1983 *Opt. Lett.* **8** 596–8
[35] Cooper N R 2008 *Adv. Phys.* **57** 539–616
[36] Graß T, Raventós D, Lewenstein M and Julià-Díaz B 2014 *Phys. Rev. B* **89** 045114